


RESEARCH

Open Access



Cross-reactive CD8⁺ T cell responses to tumor-associated antigens (TAAs) and homologous microbiota-derived antigens (MoAs)

Beatrice Cavalluzzo¹, Marie Christine Viuff², Siri Amanda Tvingsholm², Concetta Ragone¹, Carmen Manolio¹, Angela Mauriello¹, Franco M. Buonaguro³, Maria Lina Tornesello³, Francesco Izzo⁴, Alessandro Morabito⁵, Sine Reker Hadrup², Maria Tagliamonte^{1*} and Luigi Buonaguro^{1*} 

Abstract

Background We have recently shown extensive sequence and conformational homology between tumor-associated antigens (TAAs) and antigens derived from microorganisms (MoAs). The present study aimed to assess the breadth of T-cell recognition specific to MoAs and the corresponding TAAs in healthy subjects (HS) and patients with cancer (CP).

Method A library of > 100 peptide-MHC (pMHC) combinations was used to generate DNA-barcode labelled multimers. Homologous peptides were selected from the Cancer Antigenic Peptide Database, as well as Bacteroidetes/Firmicutes-derived peptides. They were incubated with CD8⁺ T cells from the peripheral blood of HLA-A*02:01 healthy individuals ($n=10$) and cancer patients ($n=16$). T cell recognition was identified using tetramer-staining analysis. Cytotoxicity assay was performed using as target cells TAP-deficient T2 cells loaded with MoA or the paired TuA.

Results A total of 66 unique pMHC recognized by CD8⁺ T cells across all groups were identified. Of these, 21 epitopes from microbiota were identified as novel immunological targets. Reactivity against selected TAAs was observed for both HS and CP. pMHC tetramer staining confirmed CD8⁺ T cell populations cross-reacting with CTA SXX2 and paired microbiota epitopes. Moreover, PBMCs activated with the MoA were shown to release IFN γ as well as to exert cytotoxic activity against cells presenting the paired TuA.

Conclusions Several predicted microbiota-derived MoAs are recognized by T cells in HS and CP. Reactivity against TAAs was observed also in HS, primed by the homologous bacterial antigens. CD8⁺ T cells cross-reacting with MAGE-A1 and paired microbiota epitopes were identified in three subjects. Therefore, the microbiota can elicit an extensive repertoire of natural memory T cells to TAAs, possibly able to control tumor growth ("natural anti-cancer vaccination"). In addition, non-self MoAs can be included in preventive/therapeutic off-the-shelf cancer vaccines with more potent anti-tumor efficacy than those based on TAAs.

*Correspondence:

Maria Tagliamonte
m.tagliamonte@istitutotumori.na.it
Luigi Buonaguro
l.buonaguro@istitutotumori.na.it

Full list of author information is available at the end of the article



© The Author(s) 2024. **Open Access** This article is licensed under a Creative Commons Attribution 4.0 International License, which permits use, sharing, adaptation, distribution and reproduction in any medium or format, as long as you give appropriate credit to the original author(s) and the source, provide a link to the Creative Commons licence, and indicate if changes were made. The images or other third party material in this article are included in the article's Creative Commons licence, unless indicated otherwise in a credit line to the material. If material is not included in the article's Creative Commons licence and your intended use is not permitted by statutory regulation or exceeds the permitted use, you will need to obtain permission directly from the copyright holder. To view a copy of this licence, visit <http://creativecommons.org/licenses/by/4.0/>. The Creative Commons Public Domain Dedication waiver (<http://creativecommons.org/publicdomain/zero/1.0/>) applies to the data made available in this article, unless otherwise stated in a credit line to the data.

Introduction

Approximately 10^{14} microbes are believed to be present in the human gastrointestinal tract. This corresponds to the number of cells and a DNA content 1,000 and 10,000 times greater than that in the human body, respectively [1]. The composition of the gut microbiota can vary during life owing to changes in diet, lifestyle, and habits. However, 90% of the species colonizing the gut microbiota belong to the *Firmicutes* and *Bacteroidetes* phyla [2, 3].

The bacteria that form the microbiota play a key role in human health. They are essential for intestinal digestion, prevention of pathogenic bacterial invasion, and regulation of the immune system [4, 5]. In addition to their physiological roles, the microbiota is actively involved in human diseases [6, 7], including tumor development and responses to treatments [8, 9]. Such a role has been mainly attributed to the production of specific metabolites, which may influence the genesis and development of cancer, as well as regulate the innate and adaptive immune responses [10–15].

A different perspective on the role of microbiota in cancer development and evolution is provided by the immunological mechanism based on the “molecular mimicry”. The latter is considered the major mechanism underlying immune disorders [16]. In particular, gut microbiota dysbiosis has been implicated in the activation of pathogenic T-cell responses, leading to gut-distal autoimmune diseases [17]. Activation of diabetogenic $CD8^+$ T cells by molecular mimicry between microbial antigens of the gut microbiota and pancreatic islet autoantigens supports the evidence that cross-reactive $CD8^+$ T cells can be elicited at the gut level with effects at distant sites [18]. Similarly, epitopes derived from microbiota (MoAs) may mimic tumor-associated antigens (TAAs) if they share identical or structurally similar amino acid residues at the same position along the epitope sequence. Therefore, the presentation of TAA-like MoAs to the immune system, in the context of MHC class I/II molecules, would elicit $CD4^+/CD8^+$ T cells cross-reacting with TAAs presented by tumor cells [19, 20].

Sporadic evidence for homology between MoAs and TAAs, together with T-cell cross-reactivity, has been previously reported [21–24]. Very recently, our group performed an unprecedented extensive analysis and found that sequence homology between TAAs and peptides from microbiota species of the *Firmicutes* and *Bacteroidetes* phyla is a frequent finding [25]. Most MoAs – TAAs paired epitopes share 6–7 identical residues or conservative substitutions along the sequence, with limited impact on the charge of the peptide. Strikingly, three of these pairs had identical sequences. Furthermore, the paired TAAs and MoAs are characterized by highly

similar or even identical structural conformations, especially in the core TCR-facing residues with identical planar and dihedral angles. Finally, the areas of interaction with both HLA and TCR mostly match, suggesting that the paired peptides can be recognized by cross-reacting T-cells [25]. This may strongly influence the fate of tumor progression and provide a novel set of antigens for the development of next-generation anti-cancer therapeutic vaccines [26].

The present study shows that circulating $CD8^+$ T cells that react with a large array of previously undescribed MoAs can be identified in both HS and CP. In addition, reactivity against TAAs was also observed in healthy individuals, suggesting previous priming by similar MoAs. Interestingly, $CD8^+$ T cells cross-reacting with MAGE-A1 and paired MoAs were identified in three subjects.

Materials and methods

Peptide identification and epitope prediction of TAAs

Tumor-associated antigen (TAAs) epitopes for HLA-A*02:01 were obtained from the Cancer Antigenic Peptide Database (<https://caped.icp.ucl.ac.be/Peptide/list>). Using the NetMHCpan 4.1 algorithm (<https://services.healthtech.dtu.dk/service.php?NetMHCpan-4.1>), these sequences were analyzed to identify the best nonamers with a predicted affinity value < 100 nM (Strong Binders, SB).

BLAST homology search and MoAs epitopes prediction

The TAAs selected as SB according to the NetMHCpan 4.1 prediction tool were submitted to BLAST for a peptide alignment search against *Firmicutes* (taxid:1239) and *Bacteroidetes* (taxid:976) taxa within the non-redundant protein sequences database (<https://blast.ncbi.nlm.nih.gov/Blast.cgi>). For sequences with a higher level of similarity, a new prediction analysis was conducted with the NetMHCstabpan 1.0 (<https://services.healthtech.dtu.dk/services/NetMHCstabpan-1.0/>), and epitopes with a predicted affinity value < 100 nM and stability > 1 h were selected.

Epitope modelling and molecular docking

The structural conformation of the predicted epitopes bound to HLA was evaluated by modifying the peptide included in the crystallized structure of HLA-A*02:01 deposited in the Protein Data Bank (<https://www.rcsb.org>). Briefly, the 1AO7 complex (PDB <https://www.rcsb.org/structure/1AO7>), which includes the HTLV-I LLFGYPVYV epitope crystallized with the HLA-A*02:01 molecule, and the α and β chains of TCR and β 2-microglobulin were used as templates. The sequence of the peptide bound to MHC was modified and replaced with the selected nonamers using PyMol software

(PyMol Molecular graphics system, version 1.8.6.2). The modified structure was then visualized using the Molsoft Mol Browser (version 3.8-7d).

Samples collection

Peripheral blood was obtained from 15 cancer patients (5 hepatocellular carcinoma, 8 lung cancer, and 2 colon cancer with liver metastasis) and 10 healthy subjects. All samples were processed at the National Cancer Institute in Naples under informed consent, as approved by the Institutional Review Board. Fresh human peripheral blood mononuclear cells (PBMCs), isolated by density gradient centrifugation using Ficoll-Hypaque, were cryopreserved at -150°C in FBS (Gibco, Thermo Fisher Scientific) plus 10% DMSO until analysis.

DNA-barcoded pMHC-multimer library preparation

All peptides were synthesized with a purity of $\geq 90\%$ (GenScript, Piscataway, NJ, USA). The lyophilized powders were reconstituted according to the manufacturer's instructions. DNA barcoded multimer libraries for selected peptides were generated as previously described by Bentzen et al. [27]. Briefly, individual peptide-MHC (pMHC) complexes were generated by incubating for 1 h with 200 μM of each peptide and 100 $\mu\text{g}/\text{mL}$ of HLA-A*02:01 MHC molecules using direct peptide loading [28]. The pMHC monomers were then coupled to a phycoerythrin (PE)- for TAAs peptides, or allophycocyanin (APC)- for MoAs-derived peptides, conjugated dextran backbone DNA barcode-labelled. Unique DNA-barcoded multimers were used to detect pMHC-specific T cells.

Staining of antigen-specific T cells with DNA-barcoded pMHC multimers

PBMC from both cohorts were thawed and washed twice in RPMI1640 medium (Fischer Scientific 72400047) and 10% fetal bovine serum (FBS, Fischer Scientific 16140071). cells were then washed once in barcode cytometry buffer (BCB; PBS+0.5% BSA+100 mg/mL herring DNA+2 mM EDTA) and incubated with DNA barcoded pMHC multimers for 15 min at 37°C , followed by incubation at 4°C for 30 min with CD8-BV480 (BD 566121) and dump channel antibodies CD4-FITC (BD 345768), CD14-FITC (BD 345784), CD19-FITC (BD 345776), CD40-FITC (Serotech MCA1590F), CD16-FITC (BD 335035), and a dead cell marker (LIVE/DEAD Fixable Near-IR, Invitrogen 2451278). The cells were washed twice with BCB, fixed in 1% paraformaldehyde (PFA), washed twice more, and resuspended in BCB. Cells were then acquired on a flow cytometer (AriaFusion, BD Biosciences); APC-pMHC multimer and double-positive PE/APC-pMHC multimer-binding CD8+ T cells were separately sorted (Suppl. Fig. 1). Sorted cells

were centrifuged for 10 min at $5000\times g$ and the cell pellet stored at -20°C .

DNA-barcode sequence analysis

DNA barcodes from the isolated cells, as well as from an aliquot of the original multimer pool (10,000 \times final dilution in the PCR reaction; used as a baseline) were amplified using a Taq PCR Master Mix kit (QIAGEN 201443) and 3 μL of forward and reverse primer (LGC Biosearch Technologies). Purified products (QIAquick PCR Purification Kit) were sequenced using PrimBio (PA, USA). DNA barcode sequencing data were processed using Barracoda software package2 (<https://services.healthtech.dtu.dk/service.php?Barracoda-1.8>). This tool identifies the DNA barcodes used in an experiment, assigns a sample ID and pMHC specificity to each barcode, calculates the number of reads and clonally reduced reads for each pMHC-associated DNA barcode, and includes statistical data processing. Fold change (FC) in read counts mapped to a given sample relative to the mean read counts mapped to triplicate baseline samples was estimated using normalization factors determined by the trimmed mean of M-values method. P-values were calculated by comparing each experiment individually to the mean baseline sample reads using a negative binomial distribution, with a fixed dispersion parameter set to 0.1. False discovery rates (FDRs) were estimated using the Benjamini-Hochberg method described by Bentzen et al. [27]. At least 1/1,000 reads associated with a given DNA barcode relative to the total number of DNA barcode reads in that given sample were set as the threshold to avoid false-positive detection of T cell responses. DNA barcodes with $\text{FDR} < 0.1\%$ (corresponding to $p < 0.001$) and $\text{Log}_2\text{FC} > 2$ over the baseline values for the total pMHC library were considered significant and true T cell responses. The T cell frequency for each significantly enriched barcode was calculated from the percentage read count of the barcode relative to the percentage of CD8+ multimer+ T cells. A non-HLA-matching healthy donor sample was included as a negative control, and any T cell recognition determined in this sample was removed from the full dataset to exclude potential non-specific pMHC binding to T cells.

T cell staining with pMHC tetramers

Specific matched peptides (TAA/microbiota) with a T cell response detected using DNA-barcode labelled multimers were selected to generate combinatorial fluorescently labelled pMHC tetramers [29, 30]. Single-fluorochrome pMHC tetramers were produced by conjugating individual pMHC complexes generated as described above to a library of fluorophore-labelled streptavidin (SA) molecules, including PE(Biolegend 405204), APC (Biolegend

405243), PE-CF594 (BD 562284), PECy7 (Biolegend 405206), BV421 (BD563259), and BV650 (BD 563855). pMHC molecules were incubated with their respective SA-conjugated fluorochromes for 30 min at 4 °C, followed by incubation with D-biotin (Sigma) (25 µM final concentration) for 20 min at 4 °C. pMHC tetramers for each specificity were generated in two colors and mixed at a 1:1 ratio before staining the cells.

PBMCs were thawed and washed with R10+10% fetal FCS. Cells were incubated with desatinib (50 nM final concentration) and 1 µL of pooled pMHC multimers per specificity for 15 min at 37 °C in 80 µL total volume. Cells were then mixed with 20 µL antibody staining solution containing CD8-BV480 (BD B566121) (final dilution 1/50), dump channel antibodies (CD4-FITC (BD 345768; final dilution 1/80), CD14-FITC (BD 345784; final dilution 1/32), CD19-FITC (BD 345776; final dilution 1/16), CD40-FITC (Serotech MCA1590F; final dilution 1/40), CD16-FITC (BD 335035; final dilution 1/64)), and a dead cell marker (LIVE/DEAD Fixable Near-IR (Invitrogen L34976; final dilution 1/1000)) and incubated for 30 min at 4 °C. Cells were washed twice in FACS buffer (PBS+2% FCS) and acquired on an LSRFortessa flow cytometer (BD Biosciences).

In vitro pre-immunization

To confirm the presence of cross-reacting CD8⁺ T cells and their increase after a re-stimulation, PBMCs were cultured in presence of SSX2-BACT2 and SSX2-BACT3 peptides. Cells were plated at a density of 2×10^6 cells/mL in 3 mL of complete medium in a 6 well plate and stimulated with peptides at a final concentration of 10 µM in presence of 10 U/mL of IL-2 (Sigma) and 25 µL/mL of ImmunoCult™ Human CD3/CD28 T Cell Activator (StemCell technologies). After 5 days, cells were harvested, centrifuged at 1200 rpm for 5 min and stained with single-fluorochrome pMHC tetramers, generated as described above, and incubated with desatinib (50 nM final concentration) and 1 µL of pooled pMHC multimers per specificity (SSX2-PE; BACT2/BACT3-FITC) for 15 min at 37 °C in 80 µL total volume. Cells were then mixed with CD8 PE-Cy7 (Life Technologies) and CD3 superbright 436 (Invitrogen) and incubated for 30 min at 4 °C. Cells were washed twice in FACS buffer (PBS+2% FCS) and acquired on an AttuneNXT flow cytometer (LifeTechnologies).

Interferon-gamma detection

PBMCs from three healthy HLA-A02:01 positive subjects were cultured in RPMI 1640 (Gibco) supplemented with 2 mM L-Glut (HyClone), 10% human serum (Sigma-Aldrich), 100 IU/ml penicillin and 100 µg/ml streptomycin (Capricorn). Cells were maintained at 37 °C in a

humidified incubator with 5% CO₂. PBMCs were seeded at 2.5×10^6 cells/ml in 3 ml in a 6 well plate and cultured in presence of IL-2 (Sigma) at a final concentration of 10 U/mL and 25 µL/mL of ImmunoCult™ Human CD3/CD28 T Cell Activator (StemCell technologies). Following 3 days incubation, the interferon-gamma (IFN-γ) production was evaluated through the IFN-γ Secretion Assay –Cell Enrichment and Detection Kit (Miltenyi Biotec). Briefly, cells were harvested, centrifuged and incubated 4 h at 37 °C with SSX2, SSX2-BACT2 and SSX2-BACT3 peptides at a final concentration of 10 µM. Unstimulated and PHA stimulated PBMCs were used, respectively, as negative and positive controls. Subsequently, cells were washed and stained with IFN-γ Catch Reagent, incubated 45 min at 37 °C, centrifuged and labelled with IFN-γ Detection Antibody (PE), CD8 PE-Cy7 (Life Technologies) and CD3 super bright 436 (Invitrogen). After 15 min incubation on ice, cells were washed, resuspended in 500 µL of cold buffer and analysed by flow cytometry (AttuneNXT-LifeTechnologies).

Flow cytometry analysis

All flow cytometry data were analyzed using the FlowJo data analysis software (version 10.8.1; FlowJo LLC). For antigen-specific T cell identification using combinatorial pMHC tetramer staining, we gated on single, live, CD3⁺, CD8⁺ lymphocytes and selected cells positive in two tetramer colors and negative in the remaining colors. For the IFN-γ detection, cells were gated as single, CD3⁺, CD8⁺ lymphocytes and double positive to CD8⁺ and IFN-γ.

Cytotoxicity assay

Cytotoxic T Lymphocytes (CTLs) were generated from HLA-A*02:01 normal donor peripheral blood mononuclear cells (PBMC). PBMCs from four healthy HLA-A02:01 positive subjects were cultured in RPMI 1640 (Gibco) supplemented with 2 mM L-Glut (HyClone), 10% human serum (Sigma-Aldrich), 100 IU/ml penicillin and 100 µg/ml streptomycin (Capricorn). Cells were seeded at 2×10^6 cells/ml in 3 ml in a 6 well plate in presence of IL-2 (Sigma) at a final concentration of 10 U/mL and 25 µL/mL of ImmunoCult™ Human CD3/CD28 T Cell Activator (StemCell technologies). PBMCs were stimulated with 10 µg of SSX2-BACT3 peptide each 3 days for 5 times, cells without peptide were used as baseline control.

For cytotoxicity assay, T2 cells (174×CEM.T2 CRL-1992-ATCC) were loaded with SSX2; SSX2-BACT2 and SSX2-BACT3 peptides at a concentration of 50 µM, incubated O/N at 27 °C, 2 h at 37 °C and with 1X Brefeldin A for 1 h and co-cultured with stimulated PBMCs for 5 h in a Target: Effector (T:E) ratio of 1:5. Specific cytotoxic

Table 1 List of TAAs and paired MoAs selected for the study

Antigen	Sequence											Aff	specie	Seq ID
	F	L	W	G	P	R	A	L	V					
MAGE-A3/12												7.65		
A3/12 BACT1						S	I					2.41	<i>Bacteroidales bacterium</i>	MBQ8420774.1
A3/12 BACT2					E	S						3.02	<i>Prevotella shahii</i>	MBF1567568.1
A3/12 BACT3							H	D				4.66	<i>Sphingobacteria bacterium</i>	TAH08235.1
A3/12 BACT4							I	G				5.24	<i>Parafilimonas terrae</i>	MBE7199410.1
A3/12 BACT5								K				6.64	<i>Chitinophagaceae bacterium</i>	MBL0883181.1
A3/12 FIRM1						A	I					3.36	<i>Clostridia bacterium</i>	MBQ1820230.1
A3/12 FIRM2							F	S				3.71	<i>Clostridia bacterium</i>	MBQ6708923.1
A3/12 FIRM3						G				L		5.24	<i>Firmicutes bacterium</i>	HHY09163.1
A3/12 FIRM4							V	M				3.15	<i>Wansuia hejianensis</i>	QNM09157.1
A3/12 FIRM5							F			I		6.28	<i>Tissierellaceae bacterium</i>	MBC8587361.1

Antigen	Sequence											Aff	specie	Seq ID
	K	V	A	E	L	V	H	F	L					
MAGE-A3												11.32		
A3 BACT1		V	L									3.31	<i>Alistipes putredinis</i>	WP_004328936.1
A3 BACT2						F	I					5.34	<i>Bacteroidetes bacterium</i>	MBS1647326.1
A3 BACT3									H	V		11.00	<i>Solirubrum puertoricensis</i>	WP_078062927.1
A3 FIRM1						I						7.1	<i>Sedimentibacter sp.</i>	MBP8691684.1
A3 FIRM2						I		M				7.41	<i>Sedimentibacter sp.</i>	MBP7221824.1
A3 FIRM3						A	I					10.43	<i>Bacillus sp. FJAT-28004</i>	WP_054028593.1
A3 FIRM4						Y	L	T		L		2.28	<i>Clostridium sporosphaeroides</i>	MBE6834566.1
A3 FIRM5						L		M				2.57	<i>Petalouisia muris</i>	TGY95779.1

Antigen	Sequence											Aff	specie	Seq ID
	G	L	Y	D	G	M	E	H	L					
MAGE-A10												6.96		
A10 BACT1			A							D		17.29	<i>Paludibacteraceae bacterium</i>	MBQ2520985.1
A10 BACT2									R			21.51	<i>Niastella sp. CF465</i>	WP_132555660.1
A10 BACT3			V				I			V		3.48	<i>Phocaeicola vulgatus</i>	WP_134985449.1
A10 BACT4							L		N			6.22	<i>Flaviumibacter petaseus</i>	WP_046368370.1
A10 FIRM1									Y	I		3.48	<i>Clostridium kluyveri</i>	WP_012101781.1
A10 FIRM2						K		I				5.01	<i>Abssiella sp. AM29-15</i>	WP_117516162.1
A10 FIRM3						M				R		5.29	<i>Eubacterium siraeum</i>	EDS01593.1
A10 FIRM4						A				E	V	2.81	<i>Lachnospiraceae bacterium</i>	HBI63224.1
A10 FIRM5						Y			D			3.33	<i>Oscillospiraceae bacterium</i>	MBQ7053643.1

Antigen	Sequence											Aff	specie	Seq ID
	K	A	S	E	K	I	F	Y	V					
SSX2												15.3		
SSX2 FIRM1							D					16.93	<i>Agathobacter sp.</i>	MBQ8518875.1
SSX2 FIRM2							A	D				9.18	<i>Agathobacter sp.</i>	MBQ6843512.1
SSX2 BACT1							Y	T				2.68	<i>Sphingobacteriaceae bacterium</i>	RYE15078.1
SSX2 BACT2								Y				4.93	<i>Bacteroidaceae bacterium</i>	MBQ6038980.1
SSX2 BACT3								A		V		10.07	<i>Bacteroidales bacterium</i>	MBQ9583024.1
SSX2 BACT4								V			L	10.49	<i>Flavobacterium sp. CG_9.1</i>	WP_196828382.1

Antigen	Sequence											Aff	specie	Seq ID
	K	V	L	E	Y	V	I	K	V					
MAGE-A1												5.83		
A1 FIRM1										R		5.57	<i>Firmicutes bacterium</i>	NLI26328.1
A1 FIRM2										D		7.39	<i>Desulfotobacterium sp. PLL0</i>	WP_206808822.1
A1 FIRM3										T		7.83	<i>Staphylococcus pettenkoferi</i>	WP_186300960.1
A1 FIRM4									I		I	13.23	<i>Tissierellales bacterium</i>	MBC7087093.1
A1 BACT1									A	L		3.04	<i>Dyadobacter sp. CECT 9623</i>	WP_215235361.1
A1 BACT2									H	L		3.6	<i>Dyadobacter luteus</i>	WP_115829840.1
A1 BACT3											A	6.6	<i>Saprosirales bacterium</i>	MBK6621957.1
A1 BACT4											E	10.97	<i>Maribacter polysiphoniae</i>	WP_109650090.1

Antigen	Sequence											Aff	specie	Seq ID
	K	V	V	E	F	L	A	M	L					
MAGE-C1												25.43		
C1 FIRM1										R	L	6.41	<i>Paenibacillus antri</i>	TLS53416.1
C1 FIRM2										L	A	10.29	<i>Lachnospiraceae bacterium</i>	MCC2147852.1
C1 FIRM3										T		11.37	<i>Lachnospiraceae bacterium</i>	MBE5922580.1
C1 BACT1										A	V	4.84	<i>Alistipes putredinis</i>	WP_195272405.1
C1 BACT2										T	L	50.96	<i>Cyclobacteriaceae bacterium</i>	MBL7846776.1
C1 BACT3										C	A	85.24	<i>Cryomorphaeae bacterium</i>	QTN38443.1

Antigen	Sequence											Aff	specie	Seq ID
	A	L	K	D	V	E	E	R	V					
MAGE-C2												239.61		
C2 FIRM1										L	S	14.52	<i>Faeciplasma gallinarum</i>	HIS24073.1
C2 FIRM2											S	23.82	<i>Loigolactobacillus jiyuensis</i>	WP_125553189.1
C2 FIRM3												52.68	<i>Eubacterium sp.</i>	MBQ7202456.1
C2 BACT1										Y		28.67	<i>Epilithonimonas bovis</i>	WP_076782989.1
C2 BACT2											D	43.24	<i>Prevotella sp.</i>	MBQ1773637.1
C2 BACT3										I		99.47	<i>Muriicola marianensis</i>	WP_188370161.1

Table 1 (continued)

The peptide sequence of each MoA is shown in relationship to the correlated TAA. Identical aa residues at a specific position along the sequence is shown as dot in green background. Different aa residues are shown in orange, if with the same chemical property, in red, if with different chemical property

activity was evaluated with Cell-mediated Cytotoxicity Assay kit (Immunochemistry Technologies).

Data processing and statistical analysis

T cell recognition data determined by DNA-barcoded pMHC multimer analysis and all peptides with negative enrichment were set to LogFC equal to zero. GraphPad Prism6 was used to generate box plots, and related statistical analysis was used to visualize the flow cytometry data. For statistical analysis, data were assumed to have a non-Gaussian distribution, and non-parametric tests were used.

Results

Selection of TAAs and MoAs

The paired TAAs and MoAs in the present study were derived from our previous analysis [25]. MAGE-A1, MAGE-A3, MAGE-A3/12, MAGE-A10, MAGE-C1, MAGE-C2, and SSX2 TAAs, together with 3–5 corresponding MoAs derived from *Firmicutes* and *Bacteroidetes* phyla were chosen (Table 1). MoAs were selected based on the predicted affinity to the same HLA allele as the corresponding TAA (HLA-A*02:01), with a maximum value lower than 100 nM. Indeed, peptides with such predicted values show 100% confirmation of HLA binding in an experimental setting based on TAP-deficient T2 cells [25, 31–34]. The overall mean of the predicted affinity values was 13.31 nM and 41 of the 53 peptides were below this value, suggesting very high binding affinity to the HLA-A*02:01 allele. The alignment of MoAs homologous to each TAA confirmed that, despite individual differences, the most predominant aa residues at each position always correspond to those in the TAA sequence (Fig. 1).

Conformation of selected TAAs and MoAs

Epitope modelling and molecular docking were performed to prove that the sequence homology between the paired TAAs and MoAs was echoed in similar peptide conformations as well as contact areas with the HLA molecule and the TCR. The analysis confirmed that regardless of the position of the amino acid substitution along the peptide sequence, MoAs may have a similar, if not identical, conformation and pattern of contact with the α and β chains of the TCR, as shown by the footprints of the paired peptides (Fig. 2; Suppl. Figs. 2–15). The

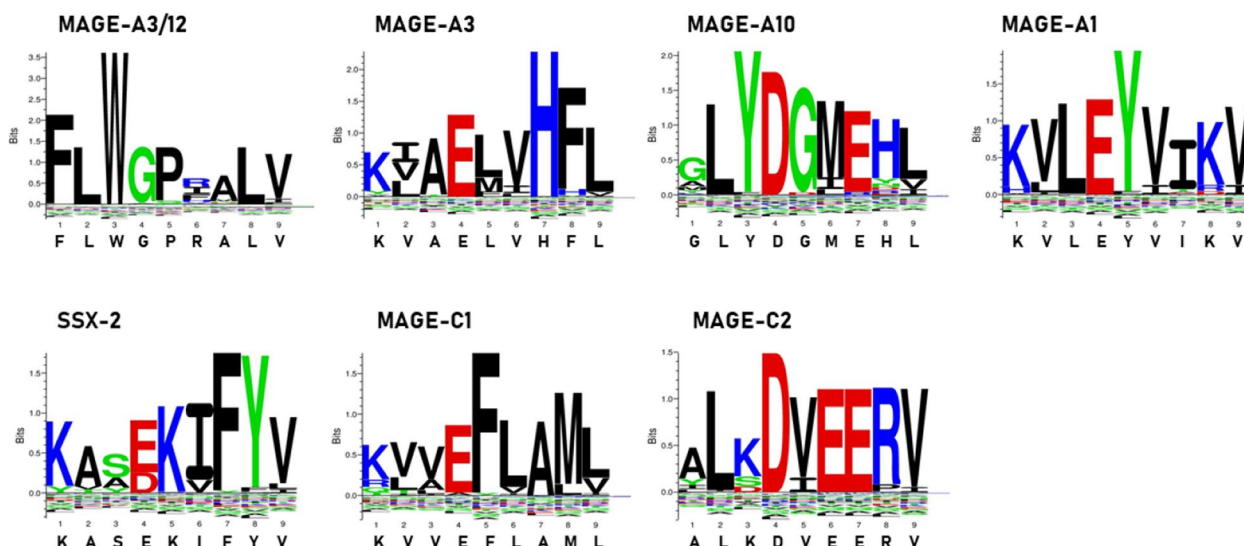


Fig. 1 SeqLogo analysis of MoAs homologous to TAA: graphical representation of amino acids belonging to the consensus sequences of MoAs aligned to the corresponding homologous TAAs. Amino acid sequences from all the microbiota-derived epitopes with homology to each TAA were piled up to build sequence logos. The height of all aminoacids at each position indicates the sequence conservation at that position, while the height of each symbol within the stack indicates the relative frequency of each aminoacid at that position (<https://services.healthtech.dtu.dk/service.php?Seq2Logo-2.0>). Different colours indicate different classes of aminoacids

best examples of identical matching are the following: 1) the KVLEYVTKV peptide derived from *Staphylococcus pettenkoferi* with a Ile - Thr substitution at position 7 compared to MAGE-A1; 2) the KIAELVHFL peptide derived from *Sedimentibacter sp.* with a Val - Ile substitution at position 2 compared to MAGE-A3; 3) the FLWGPKALV peptide derived from *Chitinophagaceae bacterium* with a Pro - Lys substitution at position 6 compared to MAGE-A3/12; 4) the GLYDGMEYI peptide derived from *Clostridium kluuyveri* with a His - Tyr and Leu - Ile substitution at position 8 and 9 compared to MAGE-A10; 5) the KTVEFLAMV peptide derived from *Lachnospiraceae bacterium* with a Val - Thr and Leu - Val substitution at position 2 and 9 compared to MAGE-C1; 6) the ALSDVEERV peptide derived from *Loigolactobacillus jiyinensis* with a Lys - Ser substitution at position 3 compared to MAGE-C2; and 7) the KVSEKIFYL peptide derived from *Flavobacterium sp. CG_9.1* with Ala - Val and Val-Leu substitutions at positions 2 and 9 compared to SSX2 (Fig. 2). In contrast, other MoAs presented substitutions that slightly or heavily affected the conformation as well as the pattern of contact with the α and β chains of the TCR (Suppl. Figs. 2–15).

Epitope analysis

DNA-barcoded peptide-major histocompatibility complex (pMHC) multimers (HLA-A*02:01) were prepared with seven selected TAAs and 53 homologous MoAs from *Firmicutes* and *Bacteroidetes* phyla. In addition, a panel of 64 peptides derived from common viruses was

constructed as an overall control of antiviral immune status. PBMCs from HLA-A*02:01 HS ($n = 10$) and CP ($n = 15$) patients were purified, incubated with DNA-barcoded pMHC multimers, and stained with a phenotype antibody panel to identify reactive CD8+ T cells [27].

The percentage of CD8+ T cells reacting against MoAs was, on average, higher in CP (95.54%) than in HS (85.18%). In contrast, the percentage of CD8+ T cells reacting to TAAs or cross-reacting with TAAs and MoAs was, on average, higher in healthy individuals (10.75% and 4.07%, respectively) than in cancer patients (2.19% and 2.28%, respectively). This difference was statistically significant for all three comparisons (Fig. 3A). Strikingly, in both groups, three subjects showed a percentage of CD8+ T cells reacting against the TAAs and cross-reacting with TAAs and MoAs well above the average value (Fig. 3A, B).

MoAs pMHC-DNA barcoding evaluation

DNA barcodes with $FDR < 0.1\%$ (corresponding to $p < 0.001$) and $Log_2FC > 2$ over the baseline values for the pMHC library were considered true and significant T-cell responses. The fraction of MoA-reacting T cells showed consistent binding to peptides homologous to MAGE-C2 (C2-BACT1, C2-BACT2, and C2-FIRM3) AND MAGE-A3/12 (A3/12-BACT1) in both tumor patients and HS. Scattered binding to peptides homologous to MAGE-C1 (C1-BACT1, C1-FIRM1, C1-FIRM2) was observed in both groups (Fig. 4A). Interestingly, while binding to such peptides was observed in scattered samples, a completely

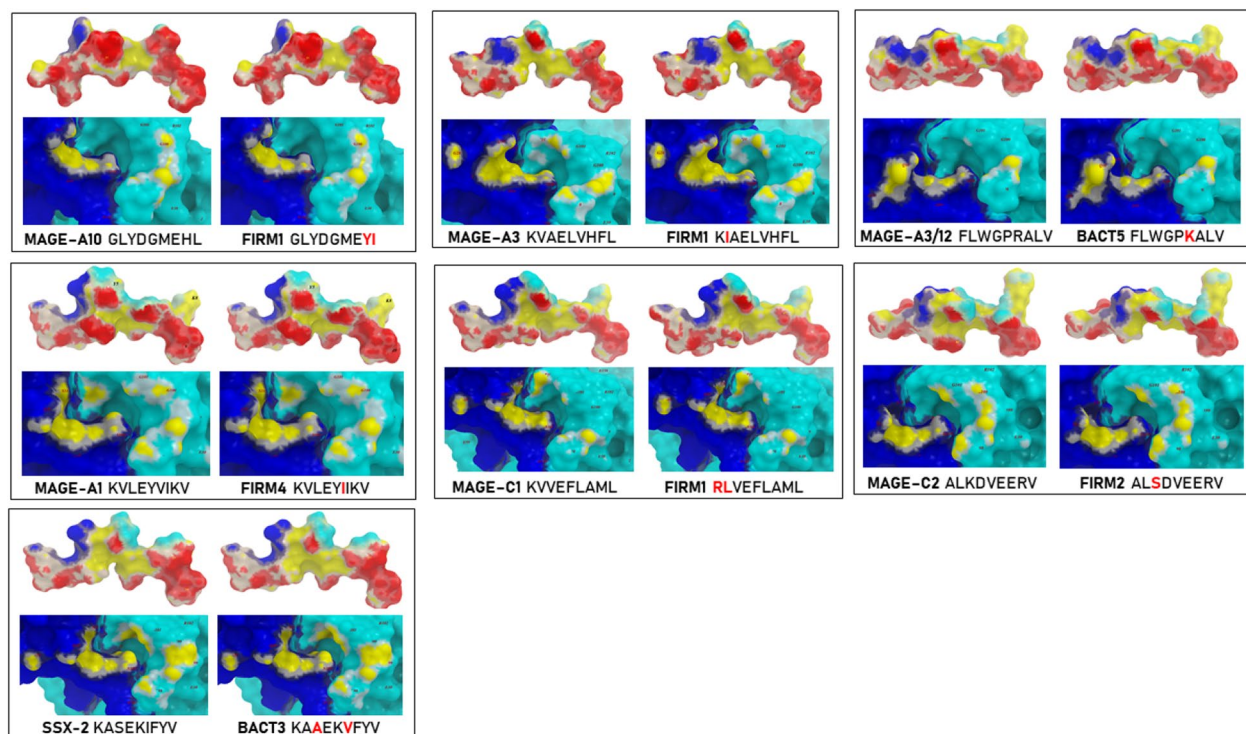


Fig. 2 Predicted 3D conformation of TAA and microbiota-derived paired peptides and peptide-TCR interaction. The surface conformation of the most similar paired HLA-A*02:01 restricted TAA and MoAs-derived peptides is shown. Residues in the microbiota-derived epitopes (FIRM = firmicutes; BACT = bacteroidetes) that differs from the TAA sequences are indicated in red color. Red areas = contact points with HLA-A molecule; blue areas = contact points with TCR α chain; Light Blue = contact points with TCR β chain. The images below the peptides show the contact sites with α and β chains of TCR (yellow areas)

different predominant pattern was observed in the fraction of cross-reacting T cells. Indeed, the peptides that were more frequently bound were those homologous to MAGE A1 and SSX2 (A1-BACT1, A1-BACT2, A1-FIRM3, A1-FIRM4) (SSX2-BACT1, SSX2-BACT2, SSX2-BACT3, SSX2-FIRM1) with an equal distribution between the two groups (Fig. 4B). The number of peptides bound by cross-reactive T cells was broadly different in both groups, ranging from 0 to 5 in healthy individuals and from 0 to 7 in tumor patients (Suppl. Fig. 16). Binding of peptides homologous to other TAAs was not observed. Consistent binding to the positive control CMVpp65 peptide was observed in of the 21/25 subjects in both groups (data not shown).

TAAs pMHC-DNA barcoding evaluation

The analysis of the fraction of double-positive T cells revealed binding to TAAs in both HS and CP, and most of this binding was specific to MAGE-A1. Three (3) HS (H-004, H-007, and H-010) showed binding to the TAAs. Binding values to MAGE-A1 peptide by H-007 and H-010 samples showed a $>2\log$ fold increase, with a high statistical significance ($p < 1 \times 10^{-6}$) (Fig. 5A).

In addition, binding values to MAGE-A1 and MAGE-C1 peptides by H-004 sample showed a statistical significance ($p < 0.005$) with a fold increase nearly reaching the $2\log$ fold increase. Seven (7) CP showed binding to TAAs (T-001, T-003, T-004, T-006, T-010, T-011, and T-015), and some of them to more than a single TAA. Binding values to MAGE-A1 peptide by T-001, T-003, T-006, and T-015 samples showed a $>2\log$ fold increase, with a high statistical significance ($p < 1 \times 10^{-6}$), while T-004 and T-011 samples showed a binding value with a statistical significance ($p < 0.005$) and a fold increase nearly reaching the $2\log$ fold increase. Binding values to MAGE-C1 peptide by T-001 and T-010 samples, to SSX2 peptide by T-004 and T-011 samples, and to MAGE-A3/12 peptide by T-011 sample showed a $>2\log$ fold increase, with a statistically significant difference ($p < 1 \times 10^{-6}$). In addition, the T-004 sample showed a binding value to A3/12 peptide with statistical significance ($p < 0.005$) and a fold increase nearly reaching the $2\log$ fold increase. Overall, the samples that reacted with more than single peptides were T-001, which bound MAGE-A1 and MAGE-C1 peptides; T-004, which bound

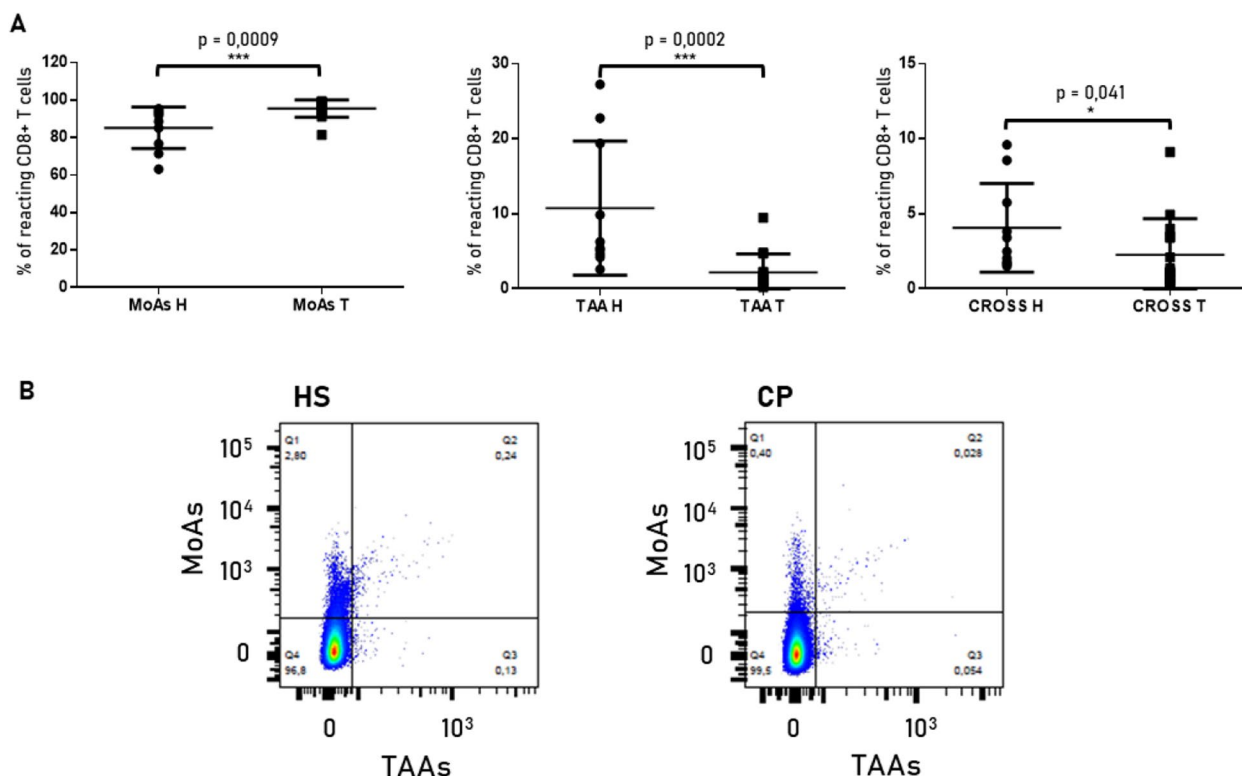


Fig. 3 CD8⁺ T cells reacting with TAAs and MoAs. The plots **(A)** show the % of sorted CD8⁺ T cells reacting against the MoAs (bacteria + viruses), the TAAs or cross-reacting with TAAs and MoAs (CROSS) (**= $p < 0,0001$, *= $p < 0,005$). **B** Representative box plot showing the % of sorted reactive CD8⁺ T cells for a healthy subject (left) and a cancer patient (right)

MAGE-A1, SSX2, and MAGE-A3/12 peptides; and T-011, which bound MAGE-A1, SSX2, and MAGE-A3/12 peptides (Fig. 5).

TAAs and MoAs cross-reactivity

According to the pMHC-DNA barcoding evaluation, two samples from the HS and three samples from the tumor patients showed double positivity for binding to homologous TAAs and MoAs with a >2log fold increase and a highly statistical significance ($p < 1 \times 10^{-6}$). In particular, the H-010, T-001, and T-006 samples showed binding to MAGE-A1 and, all three, the homologous A1-FIRM4, and H-010 bound the A1-FIRM3 (T-006), A1-BACT1 (T-001), and A1-BACT2 peptides. H-004 and T-001 samples bound to MAGE-C1 and homologous C1-FIRM1. Finally, the T-004 sample bound to SSX2 and the homologous SSX2-BACT1, SSX2-BACT2, and SSX2-BACT3 peptides (Fig. 6). In all such double reactivities, the paired TAAs and MoAs show highly similar, if not identical, conformation and contact areas to both HLA and TCR α and β chains (Fig. 2 and Suppl. Figs. 2–15).

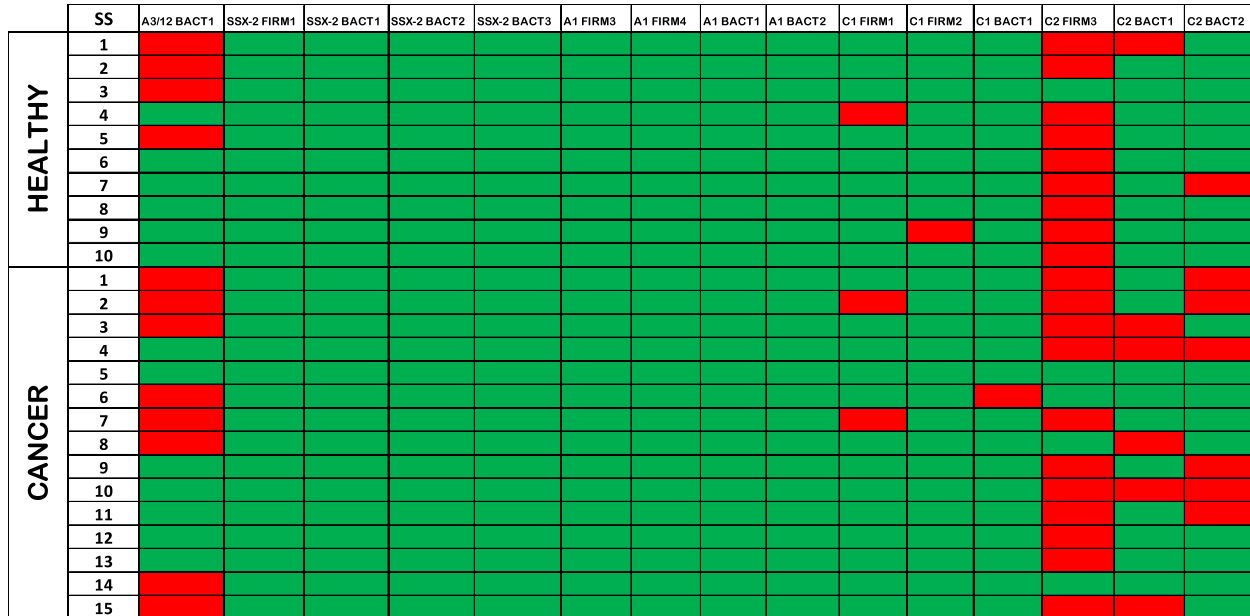
Validation of CD8⁺ T cell cross-reactivity

To confirm that the double positivity corresponded to true T cell cross-reactivity to the paired TAAs and MoAs, tetramer-staining analyses were performed.

Because of the limited availability of stored samples, the analysis was performed on sample T-004 only, which showed a broad reactivity against the SSX2 TAA and SSX2-BACT1, BACT2, and BACT3 MoAs during the DNA-barcoding screening.

Tetramer staining showed the cross-reactivity of CD8⁺ T cells with the SSX2 peptide and each of the paired MoA. Unstimulated PBMC were analyzed by flow cytometry using paired fluorescent HLA-A2/peptide tetramers and CD8-specific Abs. SSX2-, MoA-, and cross-reacting T cells were detected in the unstimulated PBMC of T-004 tumor patients. The SSX2-reacting CD8⁺ T cells were approximately 0.01%, and the MoA-reacting CD8⁺ T cells were approximately 0.004% for BACT1 and BACT2 and 0.036% for BACT3 peptide. Different levels of cross-reacting CD8⁺ T cells were observed in all three comparisons. The percentage of such CD8⁺ T cells was directly correlated with that observed for single peptide reactivity. The highest

A



B

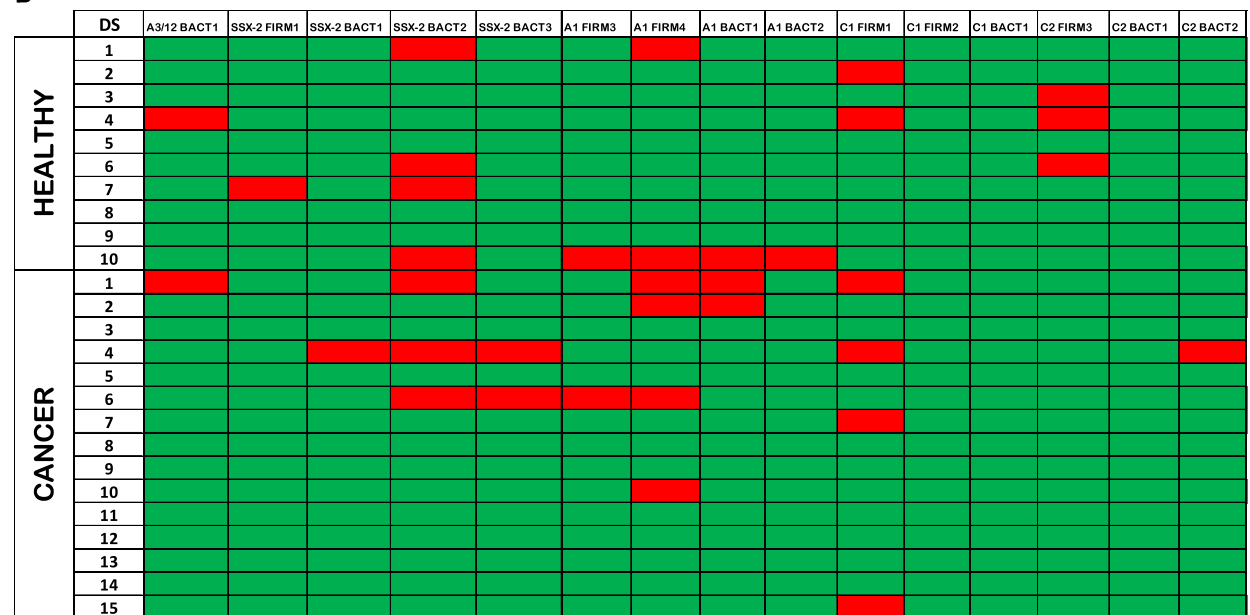


Fig. 4 Reactivity to DNA-barcoded pMHC multimer MoAs. The statistically relevant ($\text{Log}_2\text{FC} > 2$) reactivity to each peptide (column) from each subject (row) is enlightened in red. The different plots show reactivity against MoAs from the single positive (SS) (A) and from the double positive (DS) (B) sorted cell fraction

percentage of cross-reacting CD8⁺ T cells (0.011%) was observed in the SSX2/BACT3 comparison (Fig. 7A). The presence of circulating primed T cells specific for the MoAs, homologous to TAAs, was assessed by an ex vivo immunization of PBMCs. Isolated PBMCs were stimulated with SSX2-BACT2 and SSX-BACT3

peptides for 5 days and CD8⁺ T cell cross recognition of both MoAs and homologous SSX2 derived epitopes was assessed via tetramer staining. The results showed an increase in T cell recognition of both BACT2/3 and SSX2 epitopes, together with an increasing frequency of cross-reacting CD8⁺ T cells as shown in Fig. 7B.

	DS	MAGE-A3/12	SSX-2	MAGE-A1	MAGE-C1
HEALTHY	1				
	2				
	3				
	4				
	5				
	6				
	7				
	8				
	9				
	10				
CANCER	1				
	2				
	3				
	4				
	5				
	6				
	7				
	8				
	9				
	10				
	11				
	12				
	13				
	14				
	15				

Fig. 5 Reactivity to DNA-barcoded pMHC multimer TAAs. The statistically relevant (Log2FC > 2) reactivity to TAAs from each subject (row) is enlightened in red. The table shows the reactivity to TAA epitopes in both HS and CP

IFN-γ release after peptide stimulation

The activation of antigen-specific CD8+ T cells was evaluated by the production of IFN-γ after stimulation with SSX2, SSX2-BACT2 and SSX2-BACT3 peptides.

The flow cytometric analysis of IFN-γ release revealed a relevant production in all subjects (Fig. 8), with an average fold increase against the non stimulated controls

of 6.52 for SSX2, 6.48 for SSX2-BACT2 and 6.07 for SSX2-BACT3.

Cross-reactive CTL activity

The final proof of cross-reactivity was provided by assessing the cytotoxic activity of PBMCs stimulated ex vivo with the MoA-derived peptide BACT3 on TAP-deficient T2 cells loaded with SSX2, SSX2-BACT2 or SSX2-BACT3 peptides.

The results showed a cross-reactive killing activity of activated PBMCs on T2 cells presenting each of the three peptides. Interestingly, the average percentage increase of CTL activity did not reach the statistical difference in the three settings, suggesting the comparable efficient targeting of T2 cells presenting one of the paired antigens (Fig. 9).

Discussion

A high number of microorganism-derived antigens (MoAs) showing sequence and conformational homology with tumor-associated antigens (TAAs) have been recently reported, and their implication in eliciting cross-reacting anti-cancer T cells has been proposed [25, 35, 36]. In the present study, we aimed to confirm that MoAs predicted from extracellular bacteria that form the microbiota are recognized by CD8+ T cells. Consequently, the presentation of such MoAs in the context of MHC class I molecules is reasonable. Moreover, the cross-reactivity of CD8+ T cells against MoAs and homologous TAAs was investigated in patients with HS and tumors.

The selection of homologous MoAs and TAAs was based on previous observations by our group, and for each TAA, 3–5 corresponding MoAs derived from *Firmicutes* and *Bacteroidetes* phyla were chosen [25]. All selected TAAs belong to the cancer testis (CT) subgroup. In particular, antigens belonging to the Melanoma Antigen Gene family (MAGE-A1, MAGE-A3, MAGE-A3/12, MAGE-A10, MAGE-C1, MAGE-C2) and SSX2 are found to be broadly expressed in many tumor types [37, 38].

When compared to the corresponding TAA, each MoA showed a similar, if not higher, predicted affinity to the HLA molecule, despite 1–2 amino acid differences. Nevertheless, the consensus sequence derived from all

	DS	SSX-2	SSX-2 BACT1	SSX-2 BACT2	SSX-2 BACT3	MAGE-A1	A1 FIRM3	A1 FIRM4	A1 BACT1	A1 BACT2	MAGE-C1	C1 FIRM1
HEALTHY	4											
	10											
CANCER	1											
	4											
	6											

Fig. 6 Double reactivity to DNA-barcoded pMHC multimer TAAs/MoAs. The statistically relevant (Log2FC > 2) reactivity to TAAs and MoAs from each subject (row) is enlightened in red. The table shows the reactivity to homologous coupled peptides (TAA and MoAs) in both HS and CP

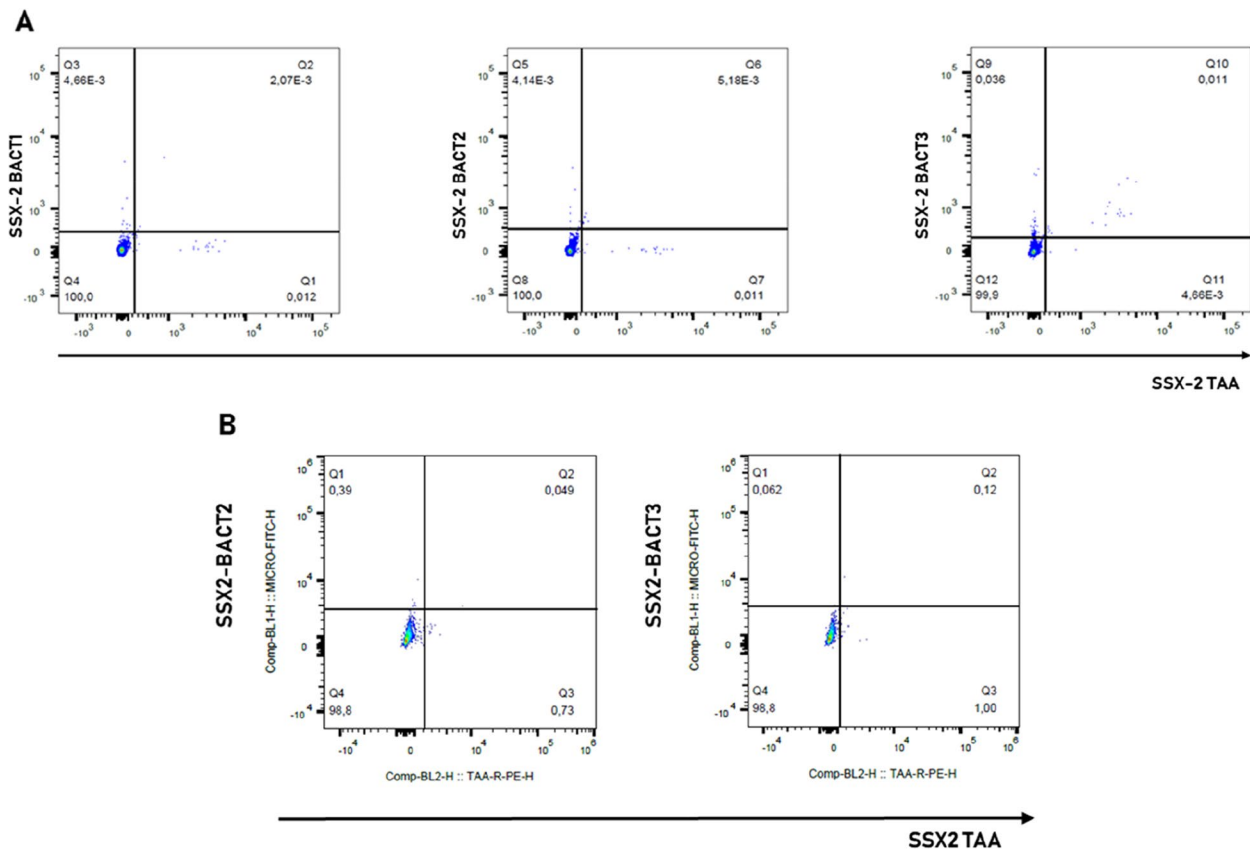


Fig. 7 **A** Cross-reactive CD8⁺ T cells in pMHC tetramer staining. Unstimulated PBMCs from sample T-004 were incubated with pMHC tetramers loaded with TAA and MoAs homologous peptides. Dot plots show the reactivity against the SSX2 peptide (PE-A) and SSX2-BACT1 (APC-A), SSX2-BACT2 (PE-CF594-A) and SSX2-BACT3 (PE-Cy7-A). **B** Cross-reactive CD8⁺ T cells in pMHC tetramer staining after in vitro pre-immunization. Cross-reactivity against the paired SSX2-BACT2/BACT3 peptides was evaluated after an in vitro pre-immunization. PBMCs were stimulated with MoAs derived epitopes and tetramer staining was used to assess the cross-recognition of homologous TAA peptide

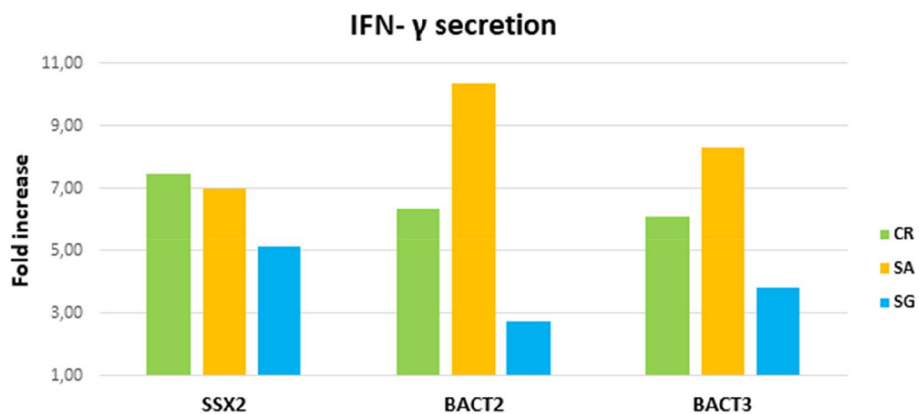


Fig. 8 IFN- γ release by CD8⁺ T cells. Secreted IFN- γ was detected using the secretion assay on viable IFN- γ ⁺ CD8⁺ T cells. The graph shows the increase in the IFN- γ production after the peptide stimulation

selected MoAs was identical to the corresponding TAA. Conformation analyses revealed highly overlapping structures between homologous TAAs and MoAs, with

indistinguishable contact areas with both HLA molecules and TCR α and β chains. Overall, this strongly suggests the induction of CD8⁺ T cells cross-reacting with TAAs

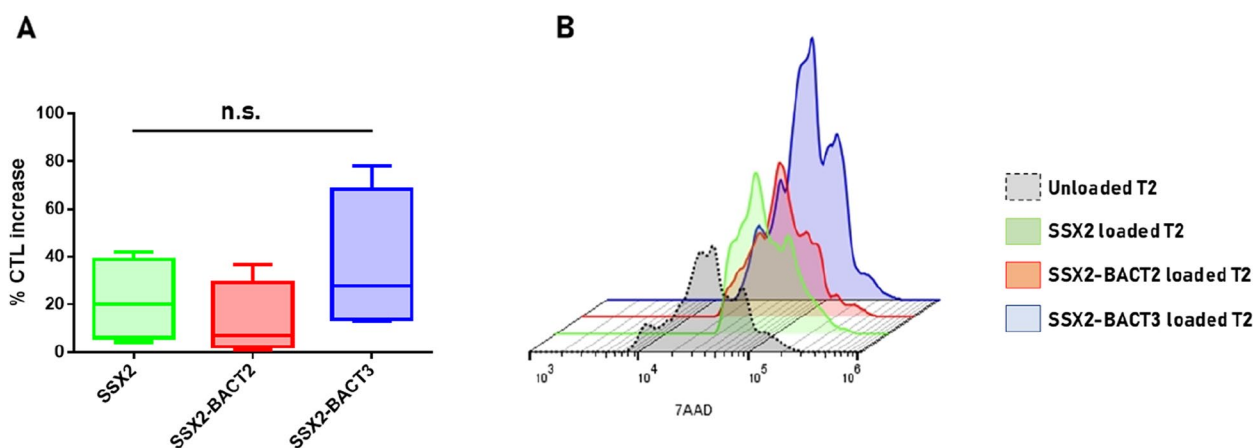


Fig. 9 CTL activity. Cytotoxic activity of PBMCs was assessed by fluorimetric assay in TAP-deficient T2 cells loaded with the indicated peptides. **A** Average percentage increase of CTL activity over T2 control cells; **B** example of layout result in a single individual, showing increase in 7AAD fluorescence intensity

and MoAs. A few exceptions to this general observation have been found, especially in the residues interacting with TCR α and β chains, when the substituting amino acid residue in the MoA was of a different chemical/structural group.

T cell binding screening was based on a panel of DNA-barcoded peptide-major histocompatibility complex (pMHC) multimers (HLA-A*02:01), including all seven selected TAAs and 53 homologous MoAs, together with 64 peptides derived from common viruses. Unstimulated CD8⁺ T cells from subjects in both experimental groups showed a high level of reactivity to MoAs, which was significantly higher in CP than in HS (95.54% vs. 85.18%). In contrast, reactivity to TAAs and cross-reactivity to MoAs and TAAs were significantly higher in HS than in CP (10.75% vs. 2.19%; 4.07% vs. 2.28%, respectively). Such unexpected observations could be reasonably explained by the priming of HS by MoAs, eliciting a T cell response that cross-reacts with the corresponding TAAs.

The evaluation of specific MoAs bound by CD8⁺ T cells showed unique patterns when sorted by single staining (T cells binding only MoAs) or double staining (T cells binding MoAs and TAAs). Single-stained (SS) T cells were found to bind MoAs homologous to MAGE-C2 and MAGE-A3/12 TAAs, in particular C2-FIRM3 (20/25 samples) and A3/12-BACT1 (12/25). Double-stained (DS) T cells, instead, were found to bind MoAs homologous to MAGE-A1 and SSX2 TAAs, in particular A1-FIRM4 (6/25 samples) and SSX2-BACT2 (7/25). The C2-FIRM3 ALKDVEEPV peptide is derived from the AMP-binding proteins of *Eubacterium* sp. and *Clostridia* bacterium. The A3/12-BACT1 FLWGSIALV peptide is derived from the cation-translocating P-type ATPase of the *Bacteroidales* genus. The A1-FIRM4 KVLEYIIKI

peptide is derived from the ATP-binding protein of the genus *Tissierellales*. Finally, the SSX2-BACT2 KAYEKI-FYV peptide was derived from an alpha/beta hydrolase of the *Bacteroidaceae* genus. None of these peptides were present in the Immune Epitope Database and Analysis Resource (iedb.org), representing the newly identified microbiota-derived MHC class I-associated epitopes. The striking consistent T cell reactivity for the C2-FIRM3 and A3/12-BACT1 peptides is likely explained by the presence of *Eubacterium* sp. and *Bacteroidales* bacterium in the universal microbiota phylogenetic core, independent of lifestyle and country of origin [39]. In particular, the *Eubacterium* spp. populations in the gut has been shown to be positively correlated with the Mediterranean diet [40].

Double-stained (DS) T cells were found to bind essentially MAGE-A1 TAA (8/25), and three subjects (H-010, T-001, and T-006) showed T cells binding both MAGE-A1 and the corresponding MoAs. Such a result may have a significant impact on a large spectrum of cancer subtypes. Indeed, MAGE-A1 is overexpressed in a significant percentage ($\geq 20\%$, on average) of different tumor types, including colon [41], melanoma [42], and lung [43], as well as in a low percentage ($\sim 10\%$) of breast [44] and liver cancers [45]. Similarly, the anecdotal observed T-cell cross-reactivity against SSX2 (T-004) or MAGE-C1 (H-004) and their homologous MoAs may be highly relevant. Indeed, SSX2 and MAGE-C1 are overexpressed in various cancers [39, 46]. We further showed that circulating T cells primed by MoAs were recalled and expanded by an in vitro immunization protocol. Such T cells reacted against TAA in a tetramer-staining analysis producing a relevant increased levels of IFN- γ . Furthermore, PBMCs ex vivo activated with the SSX2-BACT3

peptide showed a comparable cytotoxic activity against TAP-deficient T2 cells loaded with either the same peptide or the homologous SXX2 TAA or SXX2-BACT2 peptides. These results provided the conclusive proof that, indeed, T cells activated by a MoA cross-react with an homologous TAA, exerting a cytotoxic killing activity on target cells expressing the TAA.

Overall, T cell cross-reactivity against TAAs elicited by homologous MoAs may represent a potent immunological shield against a broad spectrum of cancers that can prevent tumor growth in healthy subjects or improve clinical prognosis in cancer patients. To this end, it is unfortunate that the three CP showing cross-reactive T cells in the present study were lost to follow-up, and information about clinical progression was not available.

The functional analysis in a preclinical model will definitely demonstrate the anti-tumor effect of the described cross-reactive T cells.

In conclusion, the data described provide the first large report of several MoAs, some of which have not been reported before, homologous to TAAs recognized by T cells, and cross-reactivity was observed in both HS and CP. Further studies on larger numbers of HS and CP patients will provide validation with a high potential impact on cancer immunotherapy. Indeed, non-self MoAs would become a key tool for developing preventive/therapeutic “multi-cancer” vaccine strategies with much stronger immunogenicity compared to the corresponding self-TAAs.

Supplementary Information

The online version contains supplementary material available at <https://doi.org/10.1186/s13046-024-03004-z>.

Additional file 1: Suppl. Fig. S1. Descriptive flow cytometry plots for gating strategy on healthy donors and cancer patients' PBMCs stained with DNA-barcoded pMHC multimers and surface antibody markers to sort viral/microbiome-derived (APC) and TAA/double positive (PE/PE+APC) multimer+ CD8+ T cells and to quantify multimer+ CD8+ T cells. **Suppl. Figs. S2-15.** Predicted 3D conformations of TAA and microbiota-derived paired peptides. The surface conformation of the paired TAA MoA-derived peptides is shown. Residues in the Mo epitopes that differed from the TAA sequences are indicated in red. A-Red areas = contact points with HLA-A molecule; blue areas = contact points with TCR α chain; Light Blue areas = contact points with TCR β chain. The images below the peptides show contact sites with the TCR (yellow areas). **Suppl. Fig. S16.** Diagrams show the total number of significant responses in DNA-barcoded pMHC multimers for HS (A) and CP (B).

Acknowledgements

We thank the “Associazione Giovanna Tosi per la Lotta contro i tumori” for awarding the Mobility Program Award 2021 to B.C.

Authors' contributions

BC and AM PBMCs preparation and database management; BC performed all immunological experiments and evaluations; CR and CM performed epitope prediction and conformation analysis; ALT designed the peptides; FI and AM enrolled patients and provided biological samples; MCV supported the DNA barcoded pMHC experiments; SAT supported the tetramer staining

experiments; SRH supervised all immunological experiments; MLT and FMB contributed to data analysis; MT and LB designed and coordinated the study; BC and LB drafted the manuscript.

Funding

The study was funded by the Italian Ministry of Health through Institutional “Ricerca Corrente” (Project L2/3 to LB; Project L2/13 to MTa); POR FESR 2014/2020 “Campania OncoTerapie” (LB).

Availability of data and materials

Data and material have been deposited and are publicly available at <https://doi.org/10.5281/zenodo.10817340>.

Declarations

Ethics approval and consent to participate

N/A.

Consent for publication

The corresponding author has received consent for publication.

Competing interests

The authors declare no potential conflicts of interest.

Author details

¹Innovative Immunological Models Unit, Istituto Nazionale Tumori - IRCCS - “Fond G. Pascale”, Via Mariano Semmola, 52, Naples, Italy. ²Department of Health Technology, Section of Experimental and Translational Immunology, Technical University of Denmark, Kongens Lyngby, Denmark. ³Molecular Biology and Viral Oncogenesis Unit, Istituto Nazionale Tumori - IRCCS - “Fond G. Pascale”, Naples, Italy. ⁴Hepatobiliary Surgical Oncology Unit, Istituto Nazionale Tumori - IRCCS - “Fond G. Pascale”, Naples, Italy. ⁵Thoracic Medical Oncology, Istituto Nazionale Tumori - IRCCS - “Fond G. Pascale”, Naples, Italy.

Received: 13 September 2023 Accepted: 6 March 2024

Published online: 20 March 2024

References

1. Thursby E, Juge N. Introduction to the human gut microbiota. *Biochem J*. 2017;474(11):1823–36. <https://doi.org/10.1042/BCJ20160510>. Published 2017 May 16.
2. Arumugam M, Raes J, Pelletier E, et al. Enterotypes of the human gut microbiome. *Nature*. 2011;473(7346):174–80. <https://doi.org/10.1038/nature09944>.
3. Rinninella E, Raouf P, Cintoni M, et al. What is the healthy gut microbiota composition? A changing ecosystem across age, environment, diet, and diseases. *Microorganisms*. 2019;7(1):14. <https://doi.org/10.3390/microorganisms7010014>. Published 2019 Jan 10.
4. Khosravi A, Mazmanian SK. Disruption of the gut microbiome as a risk factor for microbial infections. *Curr Opin Microbiol*. 2013;16(2):221–7. <https://doi.org/10.1016/j.mib.2013.03.009>.
5. Brestoff JR, Artis D. Commensal bacteria at the interface of host metabolism and the immune system. *Nat Immunol*. 2013;14(7):676–84. <https://doi.org/10.1038/ni.2640>.
6. Fan Y, Pedersen O. Gut microbiota in human metabolic health and disease. *Nat Rev Microbiol*. 2021;19(1):55–71. <https://doi.org/10.1038/s41579-020-0433-9>.
7. Sepich-Poore GD, Zitvogel L, Straussman R, Hasty J, Wargo JA, Knight R. The microbiome and human cancer. *Science*. 2021;371(6536):eabc4552. <https://doi.org/10.1126/science.abc4552>.
8. Routy B, Le Chatelier E, Derosa L, et al. Gut microbiome influences efficacy of PD-1-based immunotherapy against epithelial tumors. *Science*. 2018;359(6371):91–7. <https://doi.org/10.1126/science.aan3706>.
9. Vivarelli S, Salemi R, Candido S, et al. Gut microbiota and cancer: from pathogenesis to therapy. *Cancers (Basel)*. 2019;11(1):38. <https://doi.org/10.3390/cancers11010038>. Published 2019 Jan 3.

10. Paulos CM, Wrzesinski C, Kaiser A, et al. Microbial translocation augments the function of adoptively transferred self/tumor-specific CD8⁺ T cells via TLR4 signaling [published correction appears in *J Clin Invest*. 2007 Oct;117(10):3140]. *J Clin Invest*. 2007;117(8):2197–204. <https://doi.org/10.1172/JCI32205>.
11. Gur C, Ibrahim Y, Isaacson B, et al. Binding of the Fap2 protein of *Fusobacterium nucleatum* to human inhibitory receptor TIGIT protects tumors from immune cell attack. *Immunity*. 2015;42(2):344–55. <https://doi.org/10.1016/j.immuni.2015.01.010>.
12. Round JL, Mazmanian SK. Inducible Foxp3⁺ regulatory T-cell development by a commensal bacterium of the intestinal microbiota. *Proc Natl Acad Sci U S A*. 2010;107(27):12204–9. <https://doi.org/10.1073/pnas.0909122107>.
13. Shen Y, GiardinoTorchia ML, Lawson GW, Karp CL, Ashwell JD, Mazmanian SK. Outer membrane vesicles of a human commensal mediate immune regulation and disease protection. *Cell Host Microbe*. 2012;12(4):509–20. <https://doi.org/10.1016/j.chom.2012.08.004>.
14. Ivanov II, Atarashi K, Manel N, et al. Induction of intestinal Th17 cells by segmented filamentous bacteria. *Cell*. 2009;139(3):485–98. <https://doi.org/10.1016/j.cell.2009.09.033>.
15. Sprouse ML, Bates NA, Felix KM, Wu HJ. Impact of gut microbiota on gut-distal autoimmunity: a focus on T cells. *Immunology*. 2019;156(4):305–18. <https://doi.org/10.1111/imm.13037>.
16. von Herrath MG, Oldstone MB. Virus-induced autoimmune disease. *Curr Opin Immunol*. 1996;8(6):878–85. [https://doi.org/10.1016/s0952-7915\(96\)80019-7](https://doi.org/10.1016/s0952-7915(96)80019-7).
17. Levy M, Kolodziejczyk AA, Thaiss CA, Elinav E. Dysbiosis and the immune system. *Nat Rev Immunol*. 2017;17(4):219–32. <https://doi.org/10.1038/nri.2017.7>.
18. Tai N, Peng J, Liu F, et al. Microbial antigen mimics activate diabetogenic CD8⁺ T cells in NOD mice. *J Exp Med*. 2016;213(10):2129–46. <https://doi.org/10.1084/jem.20160526>.
19. Mason D. A very high level of crossreactivity is an essential feature of the T-cell receptor. *Immunol Today*. 1998;19(9):395–404. [https://doi.org/10.1016/s0167-5699\(98\)01299-7](https://doi.org/10.1016/s0167-5699(98)01299-7).
20. Garcia KC, Adams JJ, Feng D, Ely LK. The molecular basis of TCR germline bias for MHC is surprisingly simple. *Nat Immunol*. 2009;10(2):143–7. <https://doi.org/10.1038/nif.219>.
21. Loftus DJ, Castelli C, Clay TM, et al. Identification of epitope mimics recognized by CTL reactive to the melanoma/melanocyte-derived peptide MART-1 (27–35). *J Exp Med*. 1996;184(2):647–57. <https://doi.org/10.1084/jem.184.2.647>.
22. Pittet MJ, Valmori D, Dunbar PR, et al. High frequencies of naive Melan-A/MART-1-specific CD8⁺ T cells in a large proportion of human histocompatibility leukocyte antigen (HLA)-A2 individuals. *J Exp Med*. 1999;190(5):705–15. <https://doi.org/10.1084/jem.190.5.705>.
23. Dutoit V, Rubio-Godoy V, Pittet MJ, et al. Degeneracy of antigen recognition as the molecular basis for the high frequency of naive A2/Melan-a peptide multimer(+) CD8⁺ T cells in humans. *J Exp Med*. 2002;196(2):207–16. <https://doi.org/10.1084/jem.20020242>.
24. Vujanovic L, Mandic M, Olson WC, Kirkwood JM, Storkus WJ. A mycoplasma peptide elicits heteroclitic CD4⁺ T cell responses against tumor antigen MAGE-A6. *Clin Cancer Res*. 2007;13(22 Pt 1):6796–806. <https://doi.org/10.1158/1078-0432.CCR-07-1909>.
25. Ragone C, Manolio C, Mauriello A, et al. Molecular mimicry between tumor associated antigens and microbiota-derived epitopes. *J Transl Med*. 2022;20(1):316. <https://doi.org/10.1186/s12967-022-03512-6>. Published 2022 Jul 14.
26. Buonaguro L, Cerullo V. Pathogens: our allies against cancer? *Mol Ther*. 2021;29(1):10–2. <https://doi.org/10.1016/j.ymthe.2020.12.005>.
27. Bentzen AK, Marquard AM, Lyngaa R, et al. Large-scale detection of antigen-specific T cells using peptide-MHC-I multimers labeled with DNA barcodes. *Nat Biotechnol*. 2016;34(10):1037–45. <https://doi.org/10.1038/nbt.3662>.
28. Hadrup SR, Bakker AH, Shu CJ, et al. Parallel detection of antigen-specific T-cell responses by multidimensional encoding of MHC multimers. *Nat Methods*. 2009;6(7):520–6. <https://doi.org/10.1038/nmeth.1345>.
29. Andersen RS, Kvistborg P, Frøsig TM, et al. Parallel detection of antigen-specific T cell responses by combinatorial encoding of MHC multimers. *Nat Protoc*. 2012;7(5):891–902. <https://doi.org/10.1038/nprot.2012.037>. Published 2012 Apr 12.
30. Petrizzo A, Tagliamonte M, Mauriello A, et al. Unique true predicted neoantigens (TPNAs) correlates with anti-tumor immune control in HCC patients. *J Transl Med*. 2018;16(1):286. <https://doi.org/10.1186/s12967-018-1662-9>. Published 2018 Oct 19.
31. Manolio C, Ragone C, Cavalluzzo B, et al. Antigenic molecular mimicry in viral-mediated protection from cancer: the HIV case. *J Transl Med*. 2022;20(1):472. <https://doi.org/10.1186/s12967-022-03681-4>. Published 2022 Oct 15.
32. Cavalluzzo B, Mauriello A, Ragone C, et al. Novel molecular targets for hepatocellular carcinoma. *Cancers (Basel)*. 2021;14(1):140. <https://doi.org/10.3390/cancers14010140>. Published 2021 Dec 28.
33. Tagliamonte M, Mauriello A, Cavalluzzo B, et al. MHC-optimized peptide scaffold for improved antigen presentation and anti-tumor response. *Front Immunol*. 2021;12:769799. <https://doi.org/10.3389/fimmu.2021.769799>. Published 2021 Oct 20.
34. Tagliamonte M, Cavalluzzo B, Mauriello A, et al. Molecular mimicry and cancer vaccine development. *Mol Cancer*. 2023;22(1):75. <https://doi.org/10.1186/s12943-023-01776-0>. Published 2023 Apr 26.
35. Buonaguro L, Cavalluzzo B, Mauriello A, et al. Microorganisms-derived antigens for preventive anti-cancer vaccines [published online ahead of print, 2023 Jun 7]. *Mol Aspects Med*. 2023;92:101192. <https://doi.org/10.1016/j.mam.2023.101192>.
36. Schooten E, Di Maggio A, van Bergen EnHenegouwen PMP, Kijanka MM. MAGE-A antigens as targets for cancer immunotherapy. *Cancer Treat Rev*. 2018;67:54–62. <https://doi.org/10.1016/j.ctrv.2018.04.009>.
37. Türeci O, Chen YT, Sahin U, et al. Expression of S5X genes in human tumors. *Int J Cancer*. 1998;77(1):19–23. [https://doi.org/10.1002/\(sici\)1097-0215\(19980703\)77:1%3c19::aid-ijc4%3e3.0.co;2-2](https://doi.org/10.1002/(sici)1097-0215(19980703)77:1%3c19::aid-ijc4%3e3.0.co;2-2).
38. Piquer-Esteban S, Ruiz-Ruiz S, Arnau V, Diaz W, Moya A. Exploring the universal healthy human gut microbiota around the world. *Comput Struct Biotechnol J*. 2021;20:421–33. <https://doi.org/10.1016/j.csbj.2021.12.035>. Published 2021 Dec 30.
39. Ghosh TS, Rampelli S, Jeffery IB, et al. Mediterranean diet intervention alters the gut microbiome in older people reducing frailty and improving health status: the NU-AGE 1-year dietary intervention across five European countries. *Gut*. 2020;69(7):1218–28. <https://doi.org/10.1136/gutjnl-2019-319654>.
40. Mori M, Inoue H, Mimori K, et al. Expression of MAGE genes in human colorectal carcinoma. *Ann Surg*. 1996;224(2):183–8. <https://doi.org/10.1097/0000658-199608000-00011>.
41. Brasseur F, Rimoldi D, Liénard D, et al. Expression of MAGE genes in primary and metastatic cutaneous melanoma. *Int J Cancer*. 1995;63(3):375–80. <https://doi.org/10.1002/ijc.2910630313>.
42. Tajima K, Obata Y, Tamaki H, et al. Expression of cancer/testis (CT) antigens in lung cancer. *Lung Cancer*. 2003;42(1):23–33. [https://doi.org/10.1016/s0169-5002\(03\)00244-7](https://doi.org/10.1016/s0169-5002(03)00244-7).
43. Otte M, Zafrakas M, Riethdorf L, et al. MAGE-A gene expression pattern in primary breast cancer. *Cancer Res*. 2001;61(18):6682–7.
44. Zang C, Zhao Y, Qin L, et al. Distinct tumour antigen-specific T-cell immune response profiles at different hepatocellular carcinoma stages. *BMC Cancer*. 2021;21(1):1007. <https://doi.org/10.1186/s12885-021-08720-9>. Published 2021 Sep 8.
45. Bricard G, Bouzourene H, Martinet O, et al. Naturally acquired MAGE-A10- and S5X2-specific CD8⁺ T cell responses in patients with hepatocellular carcinoma. *J Immunol*. 2005;174(3):1709–16. <https://doi.org/10.4049/jimmunol.174.3.1709>.
46. Weon JL, Potts PR. The MAGE protein family and cancer. *Curr Opin Cell Biol*. 2015;37:1–8. <https://doi.org/10.1016/j.ceb.2015.08.002>.

Publisher's Note

Springer Nature remains neutral with regard to jurisdictional claims in published maps and institutional affiliations.